Bulletin of the Mineral Research and Exploration

http://bulletin.mta.gov.tr

Coulomb stress changes and magnitude-frequency distribution for Lake Van region

Hamdi ALKAN[a*] and Erdem BAYRAK[b]

[a]*Van Yüzüncü Yıl University, Faculty of Engineering, Department of Geophysics, Van, Türkiye*
[a]*Atatürk University, Earthquake Research Centre, Erzurum, Türkiye*

Research Article

Keywords:
Eastern Türkiye, Van Lake Region, Coulomb Stress, b-value, Seismotectonic.

ABSTRACT

The tectonic structure of Türkiye is under the influence of Arabian, Eurasian, African, and Anatolian plates. Lake Van region, located in eastern Türkiye, has been exposed to many devastating earthquakes in historical and instrumental periods. In this paper, using regional earthquakes, the tectonic stress variation of Lake Van region was investigated using the Coulomb stress change and the b-value distribution. 83 earthquakes that occurred between 2000 and 2020 are used to calculate the Coulomb stress change, while 17815 earthquakes that occurred between 1903 and 2021 are used to calculate the b-value distribution. Coulomb stress change gives an idea about the transfer of energy to nearby faults. Coulomb stress change and b-value distribution maps were created at different depths to model the variation of stress. The low b-values and positive Coulomb stress values were especially observed around the Van and Yeniköşk faults. On the contrary, no significant variation in stress change was observed around Süphan and Nemrut volcanoes, and high b-values were calculated in this region. Coulomb stress change and earthquake epicentral distribution are compatible and most events occurred in positive stress regions. In conclusion, stress change and b-value distribution were interpreted together and positive stress regions were revealed in the region.

Received Date: 02.07.2021
Accepted Date: 01.09.2021

1. Introduction

The Eastern Anatolian Plateau is a region located on the Alpine-Himalayan Orogenic Belt and is very active in terms of its seismicity. The active tectonics of the region are generally affected by the active collision belt that occurs as a result of the ~15 mm/year movement of the Arabian Plate to the north and the ~5 mm/year movement of the Eurasian Plate to the south (Şengör et al., 2003; Reilinger et al., 2006; Keskin, 2007; Irmak et al., 2012; Toker et al., 2017*a, b*). This collision starts approximately 11 million years ago and the boundary associated with the collision is defined as the Bitlis-Zagros Suture Zone (BZKK) (Doğan and Karakaş, 2013). The magmatic activity starts simultaneously with a new tectonic regime that develops following the collision (Alan et al., 2011). As a result of the compression deformation caused by the Eurasian and Arabian Plates, the Anatolian Plate tends to rotate counterclockwise and escape to the west. This deformation is especially dominant along the North Anatolian Fault Zone (NAFZ) and East Anatolian Fault Zone (EAFZ), which shows strike-slip fault characteristics (Keskin, 2003; Şengör et al., 2003; Bayrak et al., 2013; Reilinger et al., 2006). Right-lateral NAFZ and left-lateral EAFZ overlap at the Karlıova triple junction (Toker, 2014). To the east of the Karlıova triple junction, there are diffuse zones of deformation associated with the collision. This deformation accumulates along the NW-SE

Citation Info: Alkan, H., Bayrak, E. 2022. Coulomb stress changes and magnitude - frequency distribution for Lake Van region. Bulletin of the Mineral Research and Exploration 168, 141-156. https://doi.org/10.19111/bulletinofmre.990666

**Corresponding author: Hamdi ALKAN, hamdialkan@yyu.edu.tr*

trending dextral faults and NE-SW trending left directional faults, which represent escape tectonics in the Eastern Anatolian Block and continental lithospheric shortening along the Caucasian Thrust Zone (Toker, 2014). In the period following the continent-continental collision, active deformation caused the crustal shortening and thickening, and thus the elevation of the region (Şaroğlu and Yılmaz, 1986; Yılmaz et al., 1987; Alan et al., 2011). Lake Van Basin is located north of the BZKK, and southeast of the Karlıova triple junction (Bayrak et al., 2013).

The Van Lake Basin is a dome-shaped basin formed as a result of the tectonic activity of normal, reverse and strike-slip faults in the Eastern Anatolian compression regime. This faulting causes hydrothermal activity, intense seismicity and regional volcanism (Toker et al., 2017*a*, *b*). Lake Van Basin is approximately 1650 m above sea level and has a maximum water depth of 450 m. Süphan Volcano with an altitude of ~4400 m is located just north of Lake Van, and Nemrut Volcano with an altitude of ~3500 m is located just to the west of the lake. These volcanoes are young geological structures that were active during the Holocene time (Figure 1). Also, the metamorphic rocks and Palaeozoic aged ophiolitic units in the Bitlis Massif crop out in the south of Lake Van, and volcanic rocks and ophiolite components, young-current fluvial and lacustrine fragments and carbonates belong to the Yüksekova Complex in the east (Alan et al., 2011; Akıncı et al., 2014; Çukur et al., 2017). Volcanic and volcano-clastic rocks in the west and north of Lake Van, and Pliocene deposits and Quaternary lake sediments are settled around the city center of Van (Sumita and Schmincke, 2013; Mackenzie et al., 2016).

Lake Van consists of three deep basins, namely the Northern, Tatvan and Deveboynu basins, which are separated from each other by several ridge structures on the lake bottom (Çukur et al., 2017). Regarding the formation of the Van Lake Basin and its exact age of formation, Lahn (1948) and Degens et al. (1984) suggested that the lava flow from the Nemrut Volcano acted as a dam along the Muş Basin and was formed due to the interruption caused by the drainage of the Murat River. However, recent studies show that this is not a lava flow, but potentially a kind of pyroclastic flow, and the outlet of Lake Van was blocked much earlier than assumed (about 600.000 years ago) (Çukur et al., 2014).

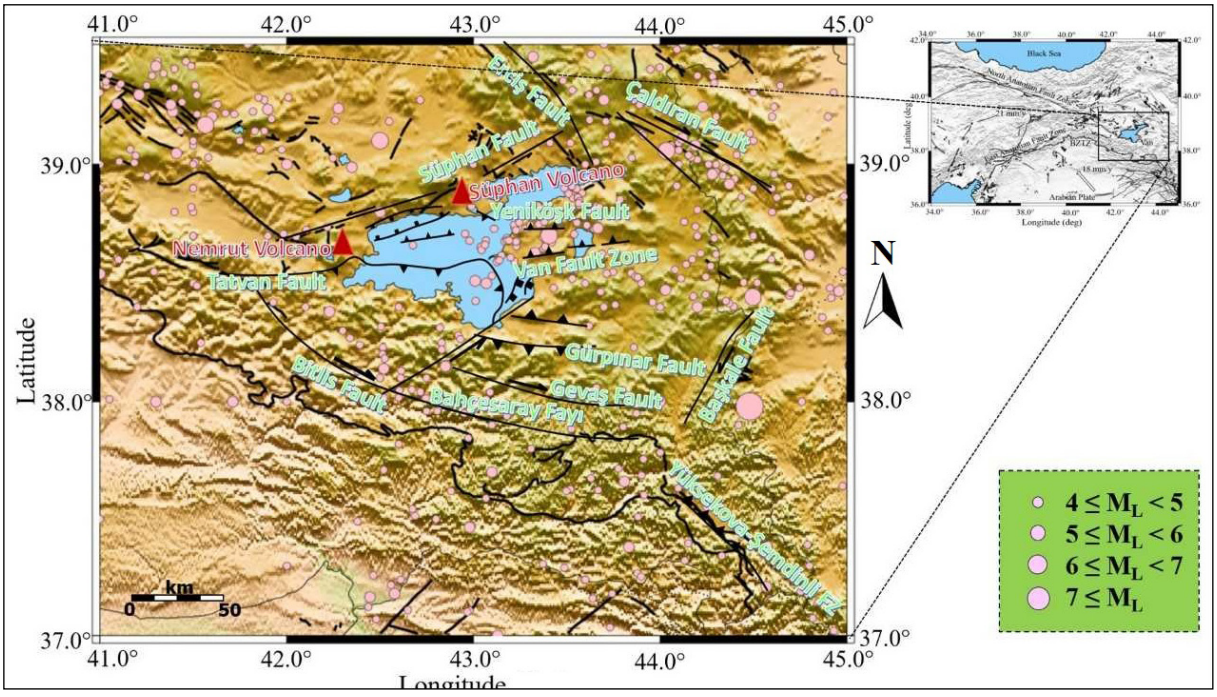

Figure 1- Seismotectonic map of the Van Lake Basin (modified from Selçuk, 2016; Emre et al., 2018 and Alkan et al., 2020). Holocone volcanoes are shown with red triangles.

The Van Lake Basin is under the influence of several active tectonic structures (Figure 1, Görür et al., 2015) Gevaş Fault and Süphan Fault located between Gevaş and Gürpınar towns, and the Çaldıran Fault and Erciş Fault located in the northeast of the lake have right-lateral strike-slip fault characteristic (Bayrak et al., 2013). The Van Fault Zone and Yeniköşk Fault, which are very close to the city center of Van, show an east-west direction reverse fault mechanism (Emre et al., 2013). Gürpınar Fault is a fault located in the south of Van and consists of three different segments. This fault is seismically active and has an east-west direction reverse and strike-slip fault mechanism (Selçuk, 2016). The Başkale Fault and Yüksekova-Şemdinli Fault Zone located in the southeast of the region are important tectonic structures. These active faults, which show a strike-slip faulting mechanism, have caused significant earthquakes (Akkaya, 2015).

The Van Lake Basin and its surroundings have been exposed to many destructive earthquakes in the historical and instrumental periods. In the historical period, the locations of 24 earthquakes with a magnitude greater than 5 and varying between V-IX have been determined (Alan et al., 2011). According to the instrumental period data, a large number of earthquakes with magnitudes between 3 and 7.3 occurred in the Van Lake Basin and its surroundings. The most important of them are; Başkale Earthquake (M=6.0) in 1908, Erciş Earthquake (Ms=5.9) in 1941, Çaldıran Earthquake in 1976 (Ms=7.3), Sütlüce Earthquake in 2005 (Ms=5.9) and the Van Earthquake that occurred in 2011 (Mw=7.2) (Akkaya, 2015; Özer, 2019; Alkan et al., 2020). 2011 Van earthquake resulted in 600 mortalities and the destruction of hundreds of buildings, rendering them unusable (Işık et al., 2017). Just after the Van Earthquake, the focal mechanism solution of which was a reverse fault, another earthquake with Ml=5.6 occurred southwest of Van Lake on 09.11.2011. It has been determined that this earthquake is independent of the Van Fault Zone, where the first earthquake occurred, and has a left-sided strike-slip mechanism on the Edremit Fault (Akıncı et al., 2014; Işık et al., 2017; Öztürk, 2017). In addition, 6284 aftershocks with magnitudes ranging from 1.7 to 5.8 occurred in the region between 23.10.2011 and 09.12.2011 (AFAD, 2011). On 23.02.2020, an earthquake (Mw=5.9) with the epicenter of Hoy (Iran) occurred at the northeastern end of the Başkale Fault. On the same day, another earthquake (Mw=5.9) occurred in the same region (AFAD, 2020*a*). Finally, an earthquake (Mw=5.4) the epicenter of which was Saray (Van) occurred on 25.06.2020 and was felt strongly in the surrounding settlements (AFAD, 2020*b*).

Coulomb stress change is very important in earthquake interactions, interpretation of future earthquakes, and assessment of seismic hazard. Also, the *b*-value calculated from the Gutenberg-Richter relationship is frequently used to display the state of the stress occurring along any fault zone (Ansari, 2016). In this study; Coulomb stress change is modeled by using focal mechanism solutions of earthquakes greater than 4.5 (Table 1) in and around the Van Lake Basin, and *b*-values are calculated using the highest probability method. Using these maps, it is aimed to determine the regional tectonic stress variation and determine the regions with the potential to produce earthquakes in the future.

2. Data

For the Coulomb stress changes, the focal mechanism results of 83 earthquakes that occurred between 2000 and 2020 in the study region were used. Table 1 shows the date, magnitude, depth, strike, rake, and dip values. According to the focal mechanism results, it is seen that strike-slip and reverse faults are active (Figure 2).

2.1. Data Used for the Gutenberg - Richter Method

The *b-value* is calculated using the AFAD DDA earthquake catalog. The catalog includes 31976 earthquakes with magnitudes (M_L) ranging from 0.7 to 7.0 that occurred between 28.04.1903 and 09.06.2021. The catalog used to calculate the *b-value* should be homogeneous, that is, of the same magnitude type (Bayrak et al., 2009; Öztürk and Bayrak, 2012; Öztürk, 2015, 2018). The AFAD catalog describes it as M_L and therefore no magnitude conversion has been done.

Another important issue in making the catalog ready for calculation is the removal of foreshocks and aftershocks from the catalog. The process of removing the foreshocks and aftershocks from an

Table 1- Focal mechanism results for earthquakes occurring in the study region (37.0°-42.0°N Latitude and 41.5°-47.0°E Longitude). The focal mechanism results of earthquakes are compiled from the AFAD website (https://deprem.afad.gov.tr/ddakatalogu).

No	Date (dd mm yy)	Latitude (°N)	Longitude (°E)	Magnitude (Mw)	Depth (km)	Strike (°)	Dip (°)	Rake (°)
1	14/12/2020 21:58:45	38.901	43.487	4.7	9.20	212.0	82.0	8.0
2	03/12/2020 05:45:19	37.999	41.712	5.0	14.02	155.0	88.0	166.0
3	16/09/2020 14:48:19	38.705	41.981	4.7	17.08	231.0	64.0	40.0
4	07/08/2020 19:20:13	38.131	42.613	4.6	6.99	331.0	83.0	171.0
5	25/06/2020 10:03:29	38.472	44.028	5.4	7.48	167.0	49.0	-85.0
6	03/04/2020 05:44:24	38.909	43.529	4.7	12.99	175.0	85.0	3.0
7	23/02/2020 16:00:29	38.450	44.502	5.9	8.10	120.0	83.0	-160.0
8	23/02/2020 05:52:57	38.436	44.489	5.9	14.90	187.0	50.0	-61.0
9	21/07/2018 06:15:13	39.038	44.153	4.5	7.52	75.0	85.0	-148.0
10	23/06/2018 03:50:03	38.623	44.300	4.7	8.48	201.0	77.0	-7.0
11	14/06/2018 15:42:21	38.941	43.555	4.5	13.66	187.0	45.0	36.0
12	01/05/2017 16:30:40	38.265	42.928	4.5	12.44	308.0	88.0	177.0
13	23/11/2016 12:14:36	38.539	43.870	4.6	9.97	305.0	76.0	167.0
14	23/01/2016 07:53:44	38.049	42.670	4.5	15.21	279.0	42.0	163.0
15	29/10/2015 09:46:39	39.119	43.743	4.8	4.90	119.0	61.0	-167.0
16	23/06/2015 22:35:20	38.681	43.179	4.5	30.45	268.0	44.0	97.0
17	18/02/2014 21:51:35	38.836	43.563	4.6	11.67	224.0	81.0	34.0
18	21/09/2013 02:15:44	38.673	43.418	4.5	17.03	252.0	42.0	50.0
19	12/06/2013 19:02:51	38.624	43.690	4.6	15.91	232.0	23.0	87.0
20	24/11/2012 16:04:28	38.833	43.572	4.5	17.53	93.0	66.0	145.0
21	05/08/2012 20:37:21	37.463	42.979	5.3	12.94	326.0	58.0	154.0
22	24/06/2012 20:07:21	38.733	43.667	5.0	23.62	96.0	42.0	89.0
23	14/06/2012 05:52:51	37.157	42.443	5.5	11.68	329.0	44.0	79.0
24	26/03/2012 10:35:33	39.234	42.276	5.0	16.96	116.0	67.0	168.0
25	24/02/2012 13:07:10	38.827	43.565	4.5	22.09	22.0	82.0	-10.0
26	17/02/2012 09:32:57	38.743	43.216	4.6	7.02	258.0	50.0	56.0

Table 1- Continued.

27	20/01/2012 09:57:37	38.703	43.497	4.5	21.32	244.0	37.0	62.0
28	06/12/2011 15:46:25	37.263	43.876	4.6	3.19	312.0	83.0	-166.0
29	06/12/2011 02:55:59	38.833	43.616	4.7	15.36	119.0	58.0	172.0
30	04/12/2011 22:15:03	38.481	43.299	4.9	12.22	32.0	86.0	2.0
31	30/11/2011 00:47:21	38.470	43.290	5.0	19.79	166.0	56.0	-58.0
32	24/11/2011 00:48:07	38.633	43.028	4.5	15.90	253.0	53.0	47.0
33	22/11/2011 03:30:35	38.609	43.207	4.5	22.95	55.0	88.0	6.0
34	21/11/2011 21:00:35	38.691	43.139	4.6	1.91	238.0	90.0	4.0
35	21/11/2011 20:55:56	38.669	43.205	4.6	22.74	82.0	42.0	97.0
36	18/11/2011 17:39:39	38.802	43.852	5.2	8.00	201.0	90.0	20.0
37	17/11/2011 12:38:31	38.867	43.569	4.5	17.10	92.0	78.0	-166.0
38	14/11/2011 22:08:14	38.703	43.083	5.1	23.32	256.0	41.0	66.0
39	14/11/2011 16:47:16	38.624	43.075	4.7	18.98	103.0	49.0	105.0
40	14/11/2011 16:31:31	38.621	43.040	4.5	19.21	95.0	45.0	90.0
41	12/11/2011 18:20:01	38.632	43.173	4.6	19.15	71.0	47.0	73.0
42	09/11/2011 20:45:38	38.464	43.253	4.5	17.74	39.0	77.0	-9.0
43	09/11/2011 19:23:34	38.438	43.282	5.6	21.47	163.0	52.0	-44.0
44	08/11/2011 22:05:50	38.719	43.077	5.4	8.36	255.0	43.0	59.0
45	07/11/2011 22:14:12	38.935	43.483	4.5	14.63	156.0	69.0	-14.0
46	07/11/2011 15:54:48	38.663	43.632	4.8	4.43	31.0	69.0	5.0
47	06/11/2011 02:43:12	38.939	43.554	4.6	11.66	9.0	81.0	30.0
48	05/11/2011 19:19:15	38.814	43.513	4.6	22.03	191.0	74.0	17.0
49	02/11/2011 11:43:02	37.253	43.900	4.8	7.78	156.0	80.0	-179.0
50	02/11/2011 04:34:21	38.884	43.590	4.8	18.03	25.0	84.0	0.0
51	01/11/2011 21:10:44	38.846	43.609	4.5	5.06	237.0	54.0	56.0
52	30/10/2011 01:55:04	38.729	43.612	4.6	22.36	31.0	73.0	-23.0
53	29/10/2011 22:24:22	38.924	43.543	4.8	16.67	199.0	90.0	-18.0
54	29/10/2011 18:45:49	38.622	43.152	4.6	13.97	80.0	42.0	110.0

Table 1- Continued.

55	28/10/2011 16:34:10	38.897	43.583	4.5	12.44	198.0	86.0	-18.0
56	27/10/2011 08:04:22	37.380	43.834	5.6	21.61	267.0	48.0	110.0
57	26/10/2011 16:19:44	38.659	43.285	4.5	1.45	35.0	89.0	-3.0
58	26/10/2011 03:16:18	38.692	43.200	4.8	20.62	222.0	57.0	70.0
59	26/10/2011 02:59:05	38.828	43.506	4.6	14.81	58.0	75.0	22.0
60	25/10/2011 15:27:13	38.826	43.566	4.5	16.01	55.0	83.0	21.0
61	25/10/2011 14:55:06	38.823	43.585	5.4	17.44	36.0	89.0	-9.0
62	24/10/2011 23:55:15	38.787	43.390	4.6	26.37	21.0	89.0	-22.0
63	24/10/2011 22:13:30	38.713	43.097	4.5	19.24	239.0	52.0	65.0
64	24/10/2011 15:28:06	38.693	43.147	4.8	18.71	215.0	70.0	25.0
65	24/10/2011 08:49:19	38.706	43.582	5.0	17.27	231.0	43.0	73.0
66	24/10/2011 04:18:45	38.680	43.310	4.5	12.58	145.0	57.0	141.0
67	23/10/2011 20:45:34	38.644	43.127	5.8	6.79	137.0	55.0	147.0
68	23/10/2011 19:43:24	38.697	43.150	4.5	7.55	228.0	52.0	-119.0
69	23/10/2011 19:06:05	38.735	43.328	5.0	22.09	252.0	34.0	65.0
70	23/10/2011 18:53:47	38.724	43.302	4.8	6.08	129.0	74.0	124.0
71	23/10/2011 18:10:44	38.629	43.192	5.0	19.81	106.0	30.0	102.0
72	23/10/2011 16:05:10	38.751	43.508	4.8	20.85	175.0	43.0	57.0
73	23/10/2011 15:57:59	38.717	43.326	4.6	21.78	63.0	43.0	100.0
74	23/10/2011 15:24:29	38.590	43.149	4.7	21.55	77.0	22.0	153.0
75	23/10/2011 13:17:03	38.811	43.467	4.7	15.41	140.0	68.0	128.0
76	23/10/2011 11:32:40	38.777	43.394	5.5	22.61	213.0	51.0	99.0
77	23/10/2011 10:56:48	38.782	43.363	5.8	19.92	305.0	71.0	-140.0
78	23/10/2011 10:41:20	38.689	43.465	6.7	19.02	98.0	66.0	88.0
79	29/05/2011 11:02:29	37.216	42.560	4.6	11.25	58.0	78.0	4.0
80	30/04/2011 15:26:03	38.183	42.525	4.5	5.00	125.0	86.0	-176.0
81	14/03/2011 18:57:09	38.601	44.171	4.7	12.47	225.0	74.0	-30.0
82	25/01/2005 16:44:16	37.622	43.703	5.9	41.2	301.0	78.0	-169.0
83	15/11/2000 15:05:37	38.410	42.950	5.2	18.0	100.0	64.0	111.0

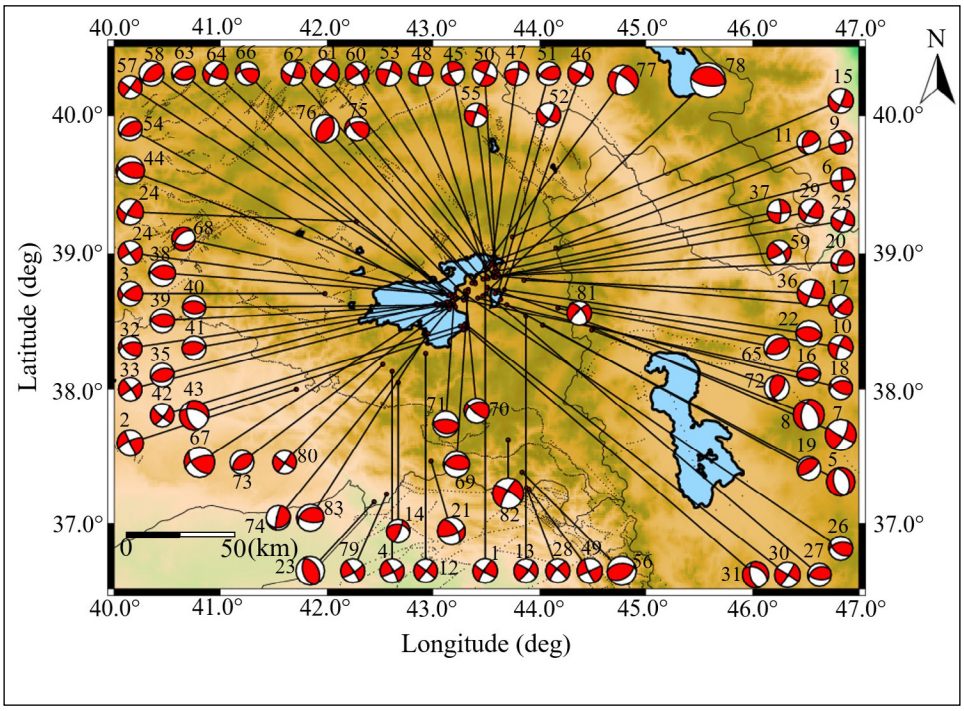

Figure 2- Fault mechanism results from major earthquakes affecting Lake Van and its surroundings. The parameters of the focal mechanism solution are given in Table 1.

earthquake catalog is known as decluster analysis. In this analysis, clustering is performed by determining a space window and a time window. There are different methods for reclustering, and the Reasenberg (1985) method, which is one of the most frequently used methods, is applied in this study. With the Reasenberg method, 14161 foreshocks and aftershocks are removed from the catalog and the final catalog consists of a total of 17815 earthquakes (Figure 3). The epicentral distribution of these earthquakes is shown in Figure 1. In Figure 3, the graph of the primary catalog and the year-earthquake number of the last catalog are shown. When this graph is examined, it is seen that there has been a significant increase in the number of earthquakes, especially after 2000, and it is thought that this is due to the increase in the number of earthquakes recorded together with the increase in earthquake stations in the region.

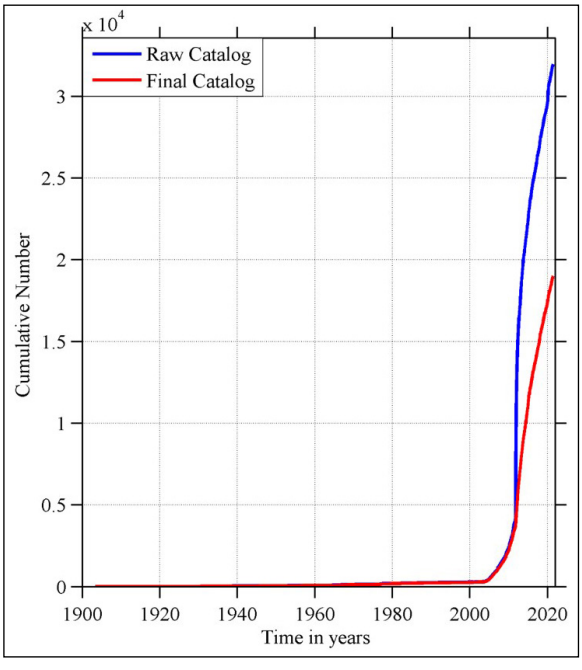

Figure 3- Cumulative number of earthquakes before and after foreshocks and aftershocks are removed from the catalog.

When the magnitude - earthquake number histogram graph of the final catalog is examined (Figure 4), it is seen that the magnitude of the majority of the earthquakes in the study region is less than 4.0. The largest earthquake that occurred in the study region was the M_L= 7.0 earthquake that occurred in 1930.

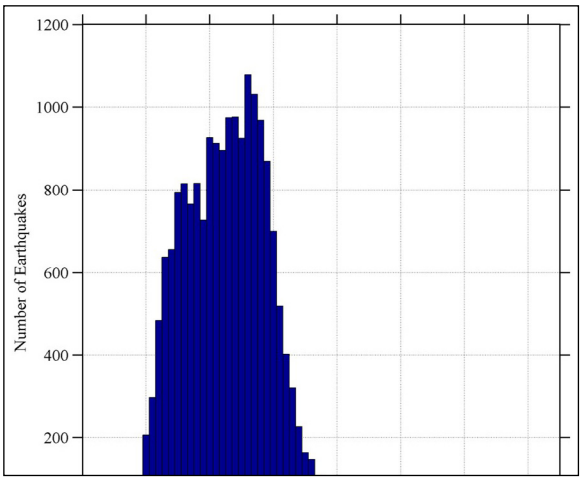

Figure 4- Magnitude histogram of the final catalog.

3. Method

3.1. Coulomb Stress Changes

The static stress change is due to the displacement of a point source or a fault, and it is necessary to multiply by the elastic stiffness to obtain the stress variation. A fault plane is a plane with a specified strike, dip, and rake in which the stress provided by a source is resolved. In the calculation of the Coulomb stress change, the shear stress component, which depends on the geometry of the fault, and the normal stress component, which depends on the subduction of the fault, are taken into account (Toda et al., 2011). Coulomb stress change depends on the geometry and sliding of an earthquake and the effective friction coefficient (Ansari, 2016; Çirmik et al., 2017). The Coulomb failure criterion is considered for the situation where the stress change is positive and is expressed by Equation 1:

$$\Delta\sigma_{cfc}=\Delta\tau_s+\mu'\Delta\sigma_{n'} \quad (1)$$

$\Delta\sigma_{cfc}$: variation of failure stress caused by shear in the source fault, $\Delta\tau_s$ variation of shear stress, $\Delta\sigma_{n'}$ normal stress variation and π: coefficient of friction on the fault. The coefficient of friction is dimensionless, ranging from 0 to 1. Poisson's ratio was chosen as 0.25, Young's modulus was 8x105 (bar) and the friction coefficient was 0.4. Positive values of the Coulomb failure criterion correspond to an increase in the probability of rupture during an earthquake, while negative values correspond to a decrease in stress (Mogi, 1962). It is assumed that Coulomb stress changes between -0.1 and +0.1 bar are sufficient to predict future earthquakes (Yadav et al., 2012). Earthquake stress changes can be used to interpret seismic hazard maps (Ahadov and Jin, 2019). In this study, Coulomb 3.3 software was used for Coulomb stress change calculations (Toda et al., 2011).

3.2. Maximum Likelihood Method

Gutenberg - Richter (1944) law, also known as the magnitude-frequency relationship, is represented by Equation 2. It has been stated that this equation is directly related to the physics of earthquake abundance (Mogi, 1962) and

$$LogN=a-bM \quad (2)$$

here, M: earthquake magnitude, N shows the cumulative number of earthquakes, a and b constant regression coefficients.

Studies have shown that the *b-value* varies depending on many different parameters. The main ones are; that the *b-value* is inversely proportional to the stress (Scholz, 1968; Wyss, 1973), directly proportional to the heterogeneity of the fault (Mogi, 1962), and directly proportional to the heat flow (Warren and Latham, 1970). It has been reported that there is an inverse proportionality between the P-wave velocity (Ogata et al., 1991) and high *b-values* are observed in aftershocks, while low *b-values* are observed in foreshocks (Suyehiro, 1964). As a result, it can be said that a low *b-value* is associated with high stress and strain, high P-wave velocity, and low heterogeneity.

There are different methods for calculating the *b-value* described by Gutenberg and Richter (1944). The most prominent of these are the least-squares and the maximum likelihood methods. With the maximum likelihood method, which is one of the most frequently used methods around the world, the *b-value* is calculated with the following formula (Aki, 1965):

$$b=\frac{1}{\log_{10}[\bar{M}-(M_{min}-\Delta m/2)]} \quad (3)$$

M_{min} is the minimum magnitude of completeness, $\bar{M}$ is the mean magnitude of earthquakes and Δm is the

magnitude resolution. The ZMAP program (Wiemer, 2001) was used to determine the Gutenberg - Richter relationship.

4. Discussion

In Figure 5, the Coulomb stress changes in the first 30 km are modeled. In especially, the positive Coulomb stress changes are shown in the region between the Van and Yenişehir Faults. In addition, positive stress values can be realized in the region between Hoy and Başkale. Negative Coulomb stress values are calculated around the Çaldıran Fault Zone. Earthquakes with $M_L \geq 4.0$ are also shown on the map to investigate the relationship between the Coulomb stress changes and the epicenters of the earthquakes. The regions of earthquake intensity usually coincide with positive Coulomb stress changes.

Figure 6 shows the Coulomb stress change results for different depths (7.5, 15, 22.5, and 30 km). Positive Coulomb stress indicates increased stress, while negative values indicate decreased stress (Olsson, 1999). Considering the stress changes at all depths, firstly positive Coulomb stress variations are observed especially around Erciş and Adilcevaz located in the north of Lake Van. This region is located in Süphan Fault and Erciş Fault. Recently, a destructive earthquake has not occurred on these faults. On the contrary, negative stress values are observed around Muradiye and Çaldıran, which are located to the east of this region. Because the Çaldıran Fault Zone has hosted destructive earthquakes in the past, the reason for the negative stress values is explained. Another important region shown in Figure 3 is the location of Van city center, which is east of Lake Van. For this region, while positive stress changes are observed at 7.5 and 15 km depths, negative stress values can be observed at increasing depths. According to these findings, it is reasonable to expect seismic activity at shallow depths in the Yeniköşk Fault and Van Fault Zone. However, the opposite situation can be mentioned for the region between Van and Hoy. Whilst negative stress values are observed at 7.5 and 15 km depths, the positive stress values are observed at 22.5 and 30 km depths.

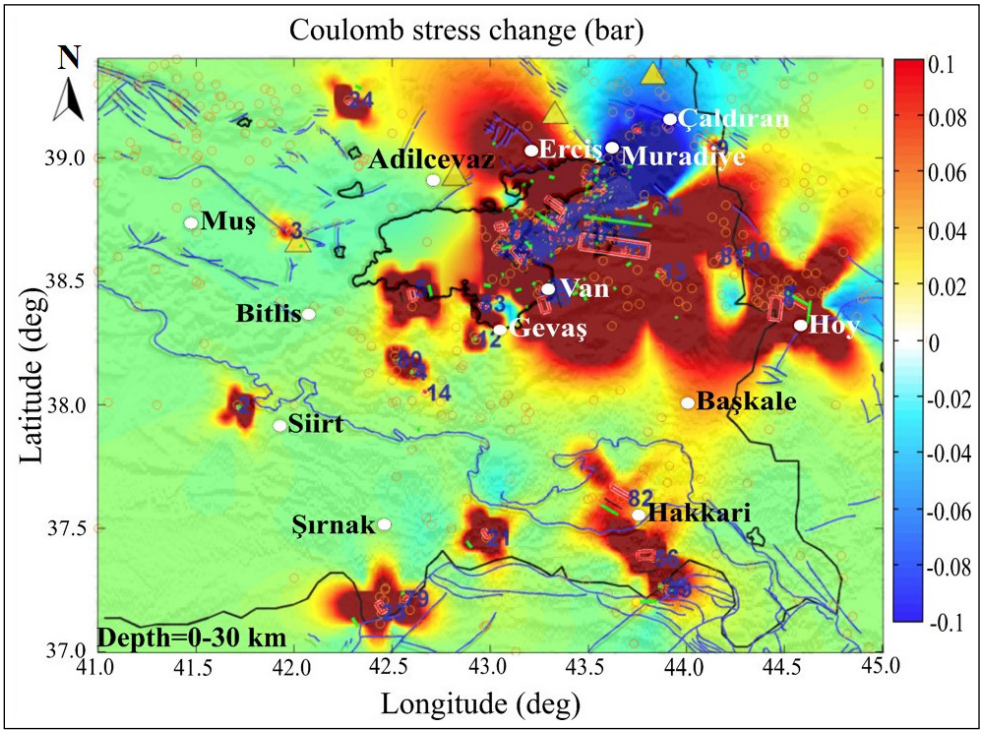

Figure 5- Coulomb stress changes calculated for a depth of 0 - 30 km (orange circles indicate the location of earthquakes greater than 4.0). The focal mechanism solutions of earthquakes were taken from the website of Kandilli Observatory and Earthquake Research Institute (KOERI, http://www.koeri.boun.edu.tr/scripts/lst0.asp).

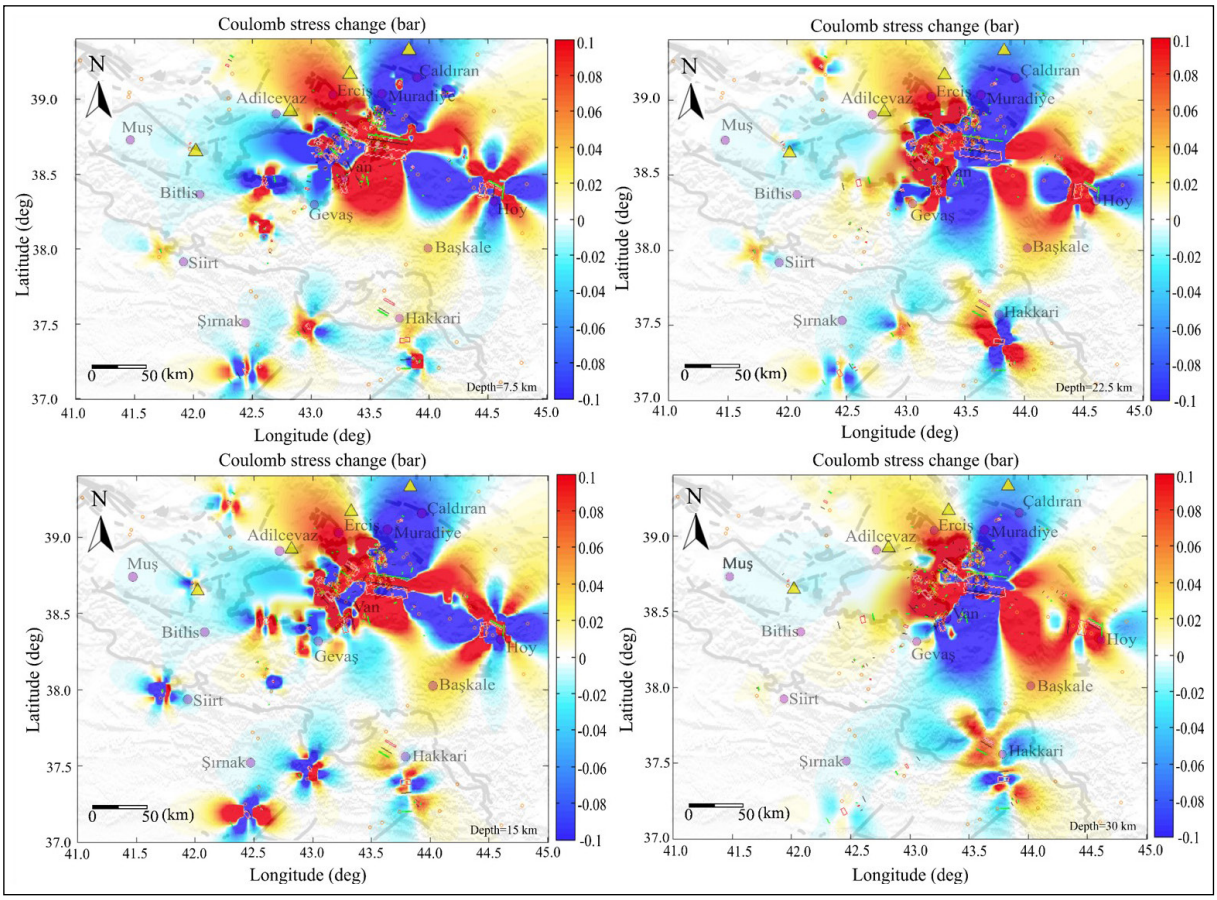

Figure 6- Coulomb stress change maps calculated for different depths. The yellow triangles represent volcanoes that are active during the Holocene.

Two earthquakes of the same magnitude (M_w= 5.9) occurred on 23.02.2020 to the northeast of the Başkale Fault. The epicentral depths of these earthquakes are 14.9 km and 8.1 km (AFAD, 2020*a*). The west of Lake Van generally has negative anomalies for each depth interval. In this region where Tatvan Fault and Bitlis Fault are located, an earthquake with a magnitude of M_w= 4.7 occurred (Table 1, Number: 3). In addition to this, when looking at the focal mechanism solutions in Figure 2, it can be seen that the potential earthquake of these faults is low. In the vicinity of Şırnak and Hakkari, located in the south of the study region, small-scale positive and negative stress anomalies are observed for all depth intervals. This stress variation shows that the Coulomb stress value is related to the small and medium earthquakes occurring in the Yüksekova - Şemdinli Fault Zone and the Southeast Anatolian Suture Zone.

Using the 0.1° × 0.1° grid interval, the regional change of the *b-value* is mapped and the closest 300 earthquakes are selected for each grid, and the minimum number of earthquakes is calculated as 20. One of the most important issues in calculating the *b-value* is the correct determination of the completeness magnitude (M_c). The method proposed by Wiemer and Wyss (2002) is used to calculate the M_c value. According to this algorithm, the number of earthquakes corresponding to the magnitude values is obtained and the magnitude value of the highest number of earthquakes is determined as M_c (Wiemer and Wyss, 2002).

The *b-value* is generally close to 1.0 in active seismic zones in different parts of the world (Frohlich and Davis, 1993). It has been stated that the *b-value* varies between 0.5 and 1.5 in different parts of the world (Wiemer and Wyss, 1997; Olsson, 1999; Öztürk and Bayrak, 2012; Öztürk, 2015, 2018).

The *b-values* obtained in this study vary between 0.5 and 1.5 (Figure 7). Figure 8 shows the standard deviations of the b-values calculated to the Maximum likelihood method. As can be clearly seen in Figure 8, standard deviation values less than 0.1 are obtained for most of the study region. This indicates that the obtained *b-values* are statistically significant. Standard deviation values greater than 1.0 are obtained for the region in the southwest of the study region. It is thought that this may be due to the low intensity of earthquakes in the region.

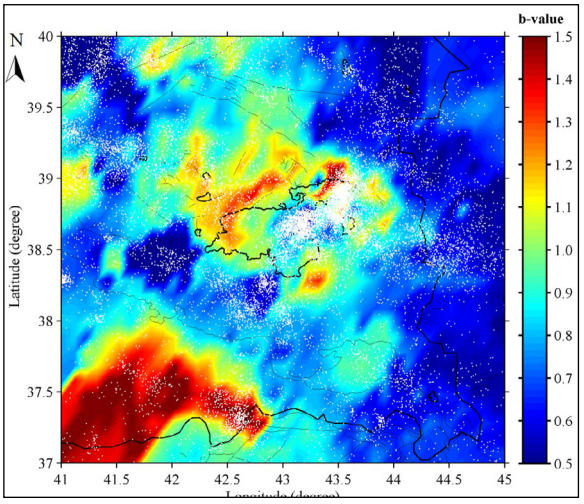

Figure 7- The *b-values* variation map calculated for the study region [white dots show the epicentral distribution of earthquakes in the catalog used in the study (URL-2)].

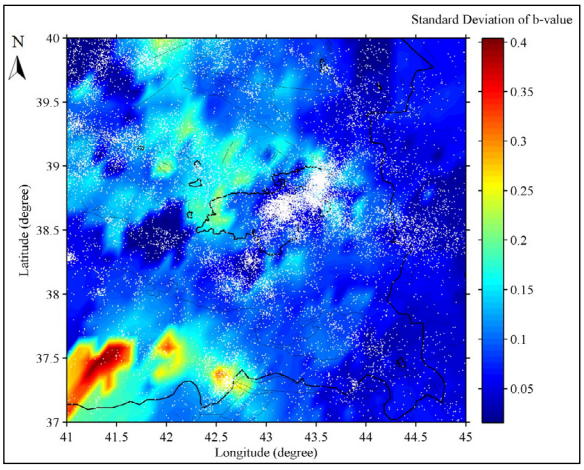

Figure 8- The standard deviation values obtained from the *b-values* [white dots depict the epicentral distribution of earthquakes in the catalog used in the study (URL-2)].

It can be seen that the *b-value* for the study region a is generally obtained as less than 1.0. Also, the highest b-values (~1.5) are obtained in the southwest of the study region. However, considering the earthquake epicenter distribution and the standard deviation map of the *b-value*, it should be said that the values obtained are not within the confidence interval since there are few earthquakes in the southwest of the study region. Relatively high *b-values* are obtained around the Süphan and Nemrut volcanoes in the NNE region of Lake Van. Cirmik (2018) calculated high heat flow values for this region. Maden and Öztürk (2015) stated that there were high negative gravity values in regions with low *b-values*. Mahatsente et al. (2018) mapped gravity anomaly values for the Eastern Anatolia region. In their study, they calculated high positive gravity anomalies for this region and these anomalies agreed with the high *b-values* in this region. As a result, it can be said that this region has a low-stress level.

Low *b-values* are also striking around the Çaldıran, Başkale, and Yüksekova-Şemdinli Faults in the east of the study region. Mahatsente et al. (2018) observed high negative gravity anomalies in this region, which is consistent with low *b-values*. Aydemir et al. (2014) obtained negative high gravity anomalies for this region in their study. It can be said that this region has a high-stress level according to the *b-value* change. Aydemir et al. (2014) determined an east-west trending discontinuity starting from the vicinity of Nemrut volcano and extending to the east of Lake Van. Lower *b-values* are obtained in the eastern section of this discontinuity compared to the western section. Büyüksaraç et al. (2021) conducted a probabilistic seismic hazard analysis in and around the Van city. They determined that the highest ground acceleration values varied between 0.24 and 0.43 g and stated that the highest danger was in the Çaldıran district, and the lowest danger was in the Gürpınar district.

Low *b-values* are striking in the vicinity of the Van Fault Zone and Yeniköşk Fault, located to the east of Lake Van. Cirmik (2018) obtained relatively high P-wave velocity values and low heat flow values for this region. Alkan et al. (2020) calculated that the depth of Moho varies between approximately 41-47 km in the Lake Van and its surroundings. They observed that the Moho discontinuity is shallower around the

Van Fault Zone and Yeniköşk Fault. The shallower Moho and low *b-values* in this region indicate a high Coulomb stress value.

Low b-values are obtained between the Bitlis Thrust Zone and Lake Van. Çırmık (2018) obtained relatively low P-wave velocities with low heat flow values for this region. While the b-values obtained in this region are compatible with the heat flow, the b-values do not show a close agreement with the P-wave velocities. Mahatsente et al. (2018) observed negative high gravity values for this region.

The relationship between the *b-value* depending on the tectonic compression and the Coulomb stress variation is very important. For this purpose, the Coulomb stress changes are calculated for the 0-30 km depth interval using the focal mechanisms shown in Table 1 (Figure 5). Positive stress changes and small *b-values* are calculated especially around the Van Fault Zone and Yeniköşk Fault. This shows that the region has a high-stress level. In addition, positive stress values and small *b-values* are calculated between the Başkale and Çaldıran Faults. No significant change in Coulomb stress change is observed around the Süphan and Nemrut Volcanoes, and high *b-values* (>1.2) are obtained in this region. These findings show the low-stress variation.

The 3-dimensional *b-value* map in the study region is created using ZMAP software. For each grid, at least 20 and the closest 200 events are selected, and a map is obtained for the 0.1° × 0.1° × 5 km grid interval. The 3-dimensional *b-value* map shown in Figure 9 is calculated using the Maximum Likelihood method. Five horizontal maps are drawn at depths of 0, 7, 5, 15, 22.5, and 30 km to examine the variation of the *b-value*. The *b-values* range from 0.5 to 1.5. According to Figure 9, the *b-value* generally decreases with increasing depth.

The *b-value* increases up to a depth of 7.5 km around the Van Fault Zone and Yeniköşk Fault. However, the *b-value* decreases after this depth. The *b-value* is obtained as 1.5 in the region where the Nemrut and Süphan volcanoes have located the northwest of Lake Van. However, the *b-value* is calculated as 1.0 at 30 km depth. Özacar et al. (2010) pointed out the existence of partial melting consisting

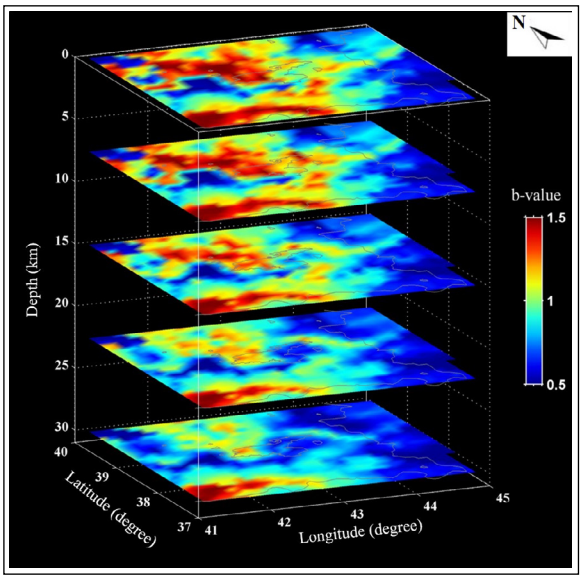

Figure 9- 3D variation of the *b-value* (maps correspond to depths of 0, 7.5, 15, 22.5, and 30 km, respectively, from top to bottom).

of young volcanic units in this region. Cirmik (2018) stated that the seismicity in this region is low and the crustal rigidity is low. According to all these results, it can be said that the stress variation of this region is low.

In the region between the Bitlis Thrust Zone and Lake Van, the *b-value* generally remains constant at 0.6 up to 15 km, and it is observed that it decreases to 0.5 after this depth. Alkan et al. (2020) determined that the P-wave velocity for this region partially increases with a depth of 30 km depth. It can be said that the high P-wave velocities are compatible with the low *b-values*.

The small *b-values* (<0.9) are founded in and around the Çaldıran Fault, Başkale Fault, and Yüksekova-Şemdinli Fault in the east of the study region. Zhu (2018) expressed this region as the Eastern Anatolia volcanic region. Zhu (2018) showed that the Vp/Vs value for this region increases with depth. On the other hand, the 1930 earthquake (M_L= 7.0), the 1976 earthquake (M_L= 6.1), and the 2020 earthquake (M_L=6.2) are reported in this region, and these earthquakes indicate that the stress values in this region are high.

The behavior of Coulomb stress changes and *b-value* at different depths are also compared in this work. Coulomb stress values generally change from negative to positive values with increasing depth. Smaller *b-values* are observed at increasing depths in the study region. In other words, it can be said that the stress level increases with increasing depths according to both values. However, positive Coulomb stress values are observed in the first 15 km around the Yeniköşk Fault located just east of Lake Van, while the negative values are obtained after this depth level. Even though this negative value, the *b-value* decreases with depth for this region. It may be useful to determine and compare the stress changes for these faults using different methods.

5. Results

Many earthquakes that caused loss of life and property in and around the Lake Van region have been reported in historical and instrumental periods. The static stress change caused by an earthquake will be useful in predicting another future earthquake on nearby faults. Coulomb stress changes are important for earthquake interactions and seismic hazard assessment. In this study, Coulomb stress changes of 83 earthquakes that occurred in and around the Lake Van region are analyzed. According to the findings of the Coulomb stress changes, it is observed that the Coulomb stress values increase around the Van, Yenişehir, Başkale, and Çaldıran Faults and it is concluded that the potential of these faults to produce earthquakes in the future is higher than the other faults in the region. In addition, the *b-value* change associated with compatibility with tectonic stress is also revealed within the scope of this study. The regions with positive Coulomb stress values show the low *b-values* and faults with high stress are revealed. In other words, the high *b-values* reflecting low-stress values are conformably obtained with negative Coulomb stress values. Finally, these parameters are calculated for different depths to model the stress change with depth and the maps of these parameters are created. It is observed that the stress generally increased with depth and these two parameters are compatible with each other. As a result, it has been shown that the positive Coulomb stress determined as a result of this study and the low *b-values* are in harmony and that these parameters can be used successfully in revealing the regions with the potential to produce earthquakes in the future.

Acknowledgements

The authors thank Republic of Türkiye Prime Ministry Disaster Emergency Management Authority Presidential of Earthquake Department (AFAD) for providing data for this study. Figures 1 and 2 were prepared using the GMT software (Wessel et al., 2013). The fault information used in the figures was digitized from the MTA drawing editor (Emre et al., 2018).

References

AFAD (T.C. İçişleri Bakanlığı, Afet ve Acil Durum Yönetimi Başkanlığı, Deprem Dairesi Başkanlığı). 2011. Van Depremi (23 Ekim 2011) raporu, Ankara.

AFAD (T.C. İçişleri Bakanlığı, Afet ve Acil Durum Yönetimi Başkanlığı, Deprem Dairesi Başkanlığı). 2020*a*. 23 Şubat 2020 Hoy (İran) Mw 5.9 depremlerine ilişkin ön değerlendirme raporu, Ankara.

AFAD (T.C. İçişleri Bakanlığı, Afet ve Acil Durum Yönetimi Başkanlığı, Deprem Dairesi Başkanlığı). 2020*b*. 25 Haziran 2020 Saray (İran) Mw 5.4 depremlerine ilişkin ön değerlendirme raporu, Ankara.

AFAD (T.C. İçişleri Bakanlığı, Afet ve Acil Durum Yönetimi Başkanlığı). https://deprem.afad.gov.tr/ddakatalogu. 01 June 2021.

Ahadov, B., Jin, S. 2019. Effects of Coulomb stress change on Mw> 6 earthquakes in the Caucasus region. Physics of the Earth and Planetary Interiors 297-106326.

Akıncı, A., Malagnini, L., Herrmann, B., Kalafat, D. 2014. High-frequency attenuation in the Lake Van region, Eastern Turkey. Bulletin of the Seismological Society of America 104(3), 1400-1409.

Aki, K. 1965. A note on the use of microseisms in determining the shallow structures of the Earth's crust. Geophysics 30, 665-666.

Akkaya, I. 2015. The application of HVSR microtremor survey method in Yüksekova (Hakkari) region, Eastern Turkey. Journal of African Earth Sciences 109, 87-95.

Alan, H., Bozkurt, E., Çağlan, D., Dirik, K., Özkaymak, Ç., Sözbilir, H., Topal, T. 2011. Van Depremleri (Tabanlı-Edremit) Raporları. Türk Mühendis

ve Mimar Odalar Birliği, Jeoloji Mühendisleri Odası, 110.

Alkan, H., Çınar, H., Oreshin, S. 2020. Lake Van (Southeastern Turkey) experiment: receiver function analyses of lithospheric structure from teleseismic observations. Pure and Applied Geophysics 177, 3891-3909.

Ansari, S. 2016. Co-seismic stress transfer and magnitude-frequency distribution due to the 2012 Varzaqan-Ahar earthquake doublets (Mw 6.5 and 6.4), NW Iran. Journal of Asian Earth Sciences 132, 129-137.

Aydemir, A., Ateş, A., Bilim, F., Büyüksaraç, A., Bektaş, O. 2014. Evaluation of gravity and aeromagnetic anomalies for the deep structure and possibility of hydrocarbon potential of the region surrounding Lake Van, Eastern Anatolia, Turkey. Surveys in Geophysics 35(2), 431-448.

Bayrak, Y., Öztürk, S., Çınar, H., Kalafat, D., Tsapanos T.M., Koravos, G.C, Leventakis, A. 2009. Estimating earthquake hazard parameters from instrumental data for different regions in and around Turkey. Engineering Geology 105(3-4), 200-210.

Bayrak, Y., Yadav, R.B.S., Kalafat, D., Tsapanos, T.M., Çınar, H., Singh, A. P., Bayrak, E., Yılmaz, Ş., Öcal, F., Koravos, G. 2013. Seismogenesis and earthquake triggering during the Van (Turkey) 2011 seismic sequence. Tectonophysics 601, 163–176.

Büyüksaraç, A., Işık, E., Harirchian, E. 2021. A case study for determination of seismic risk priorities in Van (Eastern Turkey). Earthquakes and Structures 20(4), 445–455.

Çırmık, A. 2018. Examining the crustal structures of eastern Anatolia, using thermal gradient, heat flow, radiogenic heat production and seismic velocities. Bollettino di Geofisica Teorica ed Applicata 59, 2, 117-134.

Çırmık, A., Doğru, F., Gönenç, T., Pamukçu, O. 2017. The stress/strain analysis of kinematic structure at Gülbahçe Fault and Uzunkuyu Intrusive (İzmir, Turkey). Pure and Applied Geophysics 174(3), 1425-1440.

Çukur, D., Krastel, S., Schmincke, H. U., Sumita, M., Tomonaga, Y., Çağatay, M. N. 2014. Water level changes in Lake Van, Turkey, during the past ca. 600 ka: climatic, volcanic and tectonic controls. Journal of Paleolimnology 52, 201-214.

Çukur, D., Krastel, S., Tomonaga, Y., Schmincke, H. U., Sumita, M., Meydan, A. F., Çağatay, M. N., Toker, M., Kim, S. P., Kong, G. S., Horozal, S. 2017. Structural characteristics of the Lake Van Basin, eastern Turkey, from high-resolution seismic reflection profiles and multibeam echosounder data: geologic and tectonic implications. International Journal of Earth Sciences 106, 239-253.

Degens, E. T., Wong, H. K., Kempe, S. 1984. A geological Study of Lake Van, Eastern Turkey. Geologische Rundschau 73, 701-734.

Doğan, B., Karakaş, A. 2013. Geometry of co-seismic surface ruptures and tectonic meaning of the 23 October 2011 Mw 7.1 Van earthquake (East Anatolian Region, Turkey). Journal of Structural Geology 46, 99-114.

Emre, Ö., Duman, T. Y., Özalp, S., Elmacı, H., Olgun, S., Şaroglu, F. 2013. 1/1.250.000 scale Turkey Active Fault Map. General Directorate of Mineral Research and Exploration Special Publication.

Emre, Ö., Duman, T. Y., Özalp, S., Saroglu, F., Olgun, S., Elmacı, H., Can, T. 2018. Active fault database of Turkey. Bulletin of Earthquake Engineering 16(8), 3229-3275.

Frohlich, C., Davis, S. D. 1993. Teleseismic b values; or, much ado about 1.0. Journal of Geophysical Research: Solid Earth 98(B1), 631-644.

Görür, N., Çağatay, M., Zabcı, C., Sakınç, M., Akkök, R., Şile, H., Örçen, S. 2015. The late Quaternary tectono-stratigraphic evolution of the Lake Van, Turkey. Bulletin of the Mineral Research and Exploration 151, 1-46.

Gutenberg, B., Richter, C. F. 1944. Frequency of earthquakes in California. Bulletin of the Seismological Society of America 34(4), 185-188.

Irmak, T. S., Doğan, B., Karakaş, A. 2012. Source mechanism of the 23 October 2011, Van (Turkey) earthquake (M= 7.1) and aftershocks with its tectonic implications. Earth Planets Space 64, 991-1003.

Işık, S. E., Konca, A. Ö., Karabulut, H. 2017. The seismic interactions and spatiotemporal evolution of seismicity following the October 23, 2011 M 7.1 Van, Eastern Anatolia, earthquake. Tectonophysics 702, 8-18.

Keskin, M. 2003. Magma generation by slab steepening and breakoff beneath a subduction–accretion complex: an alternative model for collision-related volcanism in Eastern Anatolia, Turkey. Geophysical Research Letters 30, 9-4.

Keskin, M. 2007. Eastern Anatolia: A hotspot in a collision zone without a mantle plume. Geological Society of America Special Paper 430, 693–722.

KOERI (Kandilli Observatory and Earthquake Research Institute). http://www.koeri.boun.edu.tr/sismo/zeqdb/. 01 June 2021.

Lahn, E. 1948. Türkiye göllerinin jeolojisi ve jeomorfolojisi hakkında bir etüd. MTA Yayınları, B(12).

Mackenzie, D., Elliott, J. R., Altunel, E., Walker, R. T., Kurban, Y.C., Schwenninger, J. L., Parsons, B. 2016. Seismotectonics and rupture process of the M 7.1 2011 Van reverse-faulting earthquake, eastern Turkey, and implications for hazard in regions of distributed shortening. Geophysical Journal International 206, 501–524.

Maden, N., Öztürk, S. 2015. Seismic b-values, bouguer gravity and heat flow data beneath Eastern Anatolia, Turkey: tectonic implications. Surveys in Geophysics 36(4), 549-570.

Mahatsente, R., Önal, G., Çemen, I. 2018. Lithospheric structure and the isostatic state of Eastern Anatolia: Insight from gravity data modelling. Lithosphere 10(2), 279-290.

Mogi, K. 1962. Study of elastic shocks caused by the fracture of heterogeneous materials and its relations to earthquake phenomena. Bulletin of the Earthquake Research Institute University of Tokyo 40(1), 125-173.

Ogata, Y., Imoto, M., Katsura, K. 1991. 3-D spatial variation of b-values of magnitude-frequency distribution beneath the Kanto District, Japan. Geophysical Journal International 104, 135-146.

Olsson, R. 1999. An estimation of the maximum b-value in the Gutenberg-Richter relation. Geodynamics 27, 547-552.

Özacar, A. A., Zandt, G., Gilbert, H., Beck, S. L. 2010. Seismic images of crustal variations beneath the East Anatolian Plateau (Turkey) from teleseismic receiver functions. Geological Society of London, Special Publications 340(1), 485-496.

Özer, Ç. 2019. Investigation of Soil Amplification in Lake Van Basin. Research Reviews in Engineering. Gece Kitaplığı, Türkiye.

Öztürk, S. 2015. Depremselliğin fraktal boyutu ve beklenen güçlü depremlerin orta vadede bölgesel olarak tahmini üzerine bir modelleme Doğu Anadolu Bölgesi, Türkiye. Gümüşhane Üniversitesi, Fen Bilimleri Enstitüsü Dergisi 5(1), 1-23.

Öztürk, S. 2017. Space-time assessing of the earthquake potential in recent years in the Eastern Anatolia region of Turkey. Earth Sciences Research Journal 21(2), 67-75.

Öztürk, S. 2018. Earthquake hazard potential in the Eastern Anatolian Region of Turkey: seismotectonic *b* and *Dc*-values and precursory quiescence *Z*-value. Frontiers of Earth Science 12(1), 215-236.

Öztürk, S., Bayrak, Y. 2012. Spatial variations of precursory seismic quiescence observed in recent years in the Eastern part of Turkey. Acta Geophysica 60(1), 92-118.

Reasenberg, P. 1985. Second-order moment of central California seismicity, 1969–1982. Journal of Geophysical Research: Solid Earth 90(B7), 5479-5495.

Reilinger, R., McClusky, S., Vernant, P., Lawrence, S., Ergintav, S., Cakmak, R., Ozener, H., Kadirov, F., Guliev, I., Stepanyan, R., Nadariya, M., Hahubia, G., Mahmoud, S., Sakr, K., ArRajehi, A., Paradissis, D., Al-Aydurs, A., Prilepin, M., Guseva, T., Evren, E., Dmitrotsa, A., Filikov, S.V., Gomez, F., Al-Ghazzi, R., Karam, G. 2006. GPS constraints on continental deformation in the Africa-Arabia-Eurasia continental collision zone and implications for the dynamics of plate interactions. Journal of Geophysical Research Solid Earth 111(B5), B05411.

Scholz, C. H. 1968. The frequency-magnitude relation of microfracturing in rock and its relation to earthquakes. Bulletin of the Seismological Society of America 58(1), 399-415.

Selçuk, A. S. 2016. Evaluation of the relative tectonic activity in the eastern Lake Van basin, East Turkey. Geomorphology 270, 9-21.

Sumita, M., Schmincke, H. U. 2013. Impact of volcanism on the evolution of Lake Van II: temporal evolution of explosive volcanism of Nemrut Volcano (eastern Anatolia) during the past ca. 0.4 Ma. Journal of Volcanology and Geothermal Research 253, 15–34.

Suyehiro, S. 1964. Foreshocks and aftershocks accompanying a perceptible earthquake in central Japan. Papers in Meteorology and Geophysics 15, 71-88.

Şaroğlu, F., Yılmaz, Y. 1986. Doğu Anadolu'da Neotektonik Dönemdeki Jeolojik Evrim ve Havza Modelleri. Maden Tetkik ve Arama Genel Müdürlüğü, Jeoloji Etütleri Dairesi, Ankara.

Şengör, A. M. C., Özeren, S., Genç, T., Zor, E. 2003. East Anatolian high plateau as a mantle-supported, north-south shortened domal structure. Geophysical Research Letters 30, 4.

Toda, S., Stein, R. S., Sevilgen, V., Lin, J. 2011. Coulomb 3.3 graphic-rich deformation and stress-change software for earthquake, tectonic, and volcano research and teaching-user guide. United State Geological Survey, Open-File Report, 1060.

Toker, M. 2014. Discrete characteristics of the aftershock sequence of the 2011 Van Earthquake. Journal of Asian Earth Sciences 92, 168-186.

Toker, M., Şengör, A. M. C., Schluter, F. D., Demirbağ, E., Çukur, D., Imren, C., Niessen, F., PaleoVan-working Group. 2017*a*. The structural elements and tectonics of the Lake Van basin (Eastern Anatolia) from multi-channel seismic reflection profiles. Journal of African Earth Sciences 129, 165-178.

Toker, M., Pınar, A., Tur, H. 2017*b*. Source mechanisms and faulting analysis of the aftershocks in the Lake Erçek area (Eastern Anatolia, Turkey) during the 2011 Van event (Mw 7.1): implications for the regional stress field and ongoing deformation processes. Journal of Asian Earth Sciences 150, 73–86.

Warren, N. W., Latham, G. V. 1970. An experimental study of thermally induced microfracturing and its relation to volcanic seismicity. Journal of Geophysical Research 75(23), 4455-4464.

Wessel, P., Smith, W. H. F., Scharroo, R., Luis, J. F., Wobbe, F. 2013. Generic Mapping Tools: Improved version released. EOS, Transactions American Geophysical Union 94, 409-410.

Wiemer, S. 2001. A software package to analyze seismicity: ZMAP. Seismological Research Letters 72(3), 373-382.

Wiemer, S., Wyss, M. 1997. Mapping the frequency-magnitude distribution in asperities: An improved technique to calculate recurrence times?. Journal of Geophysical Research: Solid Earth 102(B7), 15115-15128.

Wiemer, S., Wyss, M. 2002. Mapping spatial variability of the frequency-magnitude distribution of earthquakes. In Advances in Geophysics 45, 259.

Wyss, M. 1973. Towards a physical understanding of the earthquake frequency distribution. Geophysical Journal of the Royal Astronomical Society 31(4), 341-359.

Yadav, R. B. S., Gahalaut, V. K., Chopra, S., Shan, B. 2012. Tectonic implications and seismicity triggering during the 2008 Baluchistan, Pakistan earthquake sequence. Journal of Asian Earth Sciences 45, 167–178.

Yılmaz, Y., Şaroğlu, F., Güner, Y. 1987. Initiation of the Neomagmatism in East Anatolia. Tectonophysics 134, 177-199.

Zhu, H. 2018. High Vp/Vs ratio in the crust and uppermost mantle beneath volcanoes in the Central and Eastern Anatolia. Geophysical Journal International 214(3), 2151-2163.